



Gas phase 2-propanol degradation using titania photocatalysts: Study of the quantum efficiency

Mario J. Muñoz-Batista^a, Uriel Caudillo-Flores^b, Francisco Ung-Medina^b, Ma. del Carmen Chávez-Parga^b, José A. Cortés^{b,*}, Anna Kubacka^{a,*}, Marcos Fernández-García^a

^a Instituto de Catálisis y Petroleoquímica, CSIC, C/Marie Curie, 2, 28049 Madrid, Spain

^b Facultad de Ingeniería Química, Universidad Michoacana de San Nicolás de Hidalgo, Av. Francisco J. Mújica S/N, 58030 Morelia, Michoacán, Mexico

ARTICLE INFO

Article history:

Received 1 June 2016

Received in revised form 29 July 2016

Accepted 3 August 2016

Available online 3 August 2016

Keywords:

Anatase

Rutile

Titania

Degradation

Quantum efficiency and yield

UV

Sunlight

ABSTRACT

A series of TiO_2 samples, prepared by a microwave assisted method followed by spray drying and subjected to further calcination, were tested in gas-phase photodegradation of 2-propanol under UV and Sunlight-type illumination conditions. Samples were characterized using X-ray diffraction, porosimetry, UV-vis and Photoluminescence spectroscopies. This physico-chemical characterization was completed with the in-situ analysis of the sample behavior under illumination conditions using infrared spectroscopy. The photochemical behavior of the samples was analyzed through their reaction rate and particularly efficiency parameters, the later measured as both the apparent and true quantum efficiency. To calculate the efficiency in quantitative basis we carried out a complete analysis of the light-matter interaction in the reaction system as well as the chemical response of the catalysts measuring reaction activity and selectivity. The study measures the differences observed among the most common (including the apparent and true quantum efficiency) approximations used to calculate the efficiency parameter providing evidence that they can differ in a factor of 2–4 and shows that optimum performance in our titania-based catalysts is obtained in presence of anatase-rutile interface contact. However, the analysis of the true quantum efficiency demonstrates that this is not exclusively based in the well-known effect of such interface in charge recombination but also depends critically on the variation of the optical properties of the catalytic solids through the series.

© 2016 Elsevier B.V. All rights reserved.

1. Introduction

The environmental degradation as well as specific human health problems related to or encountered in the industrial era have forced to the implementation of technologies aiming at limiting the generation of pollutants and/or mitigating the noxious effects derived from their presence at the environment [1]. Advanced oxidation processes and particularly heterogeneous photocatalysis have evolved as powerful technologies to facilitate the control and elimination of pollutants [2,3]. Heterogeneous photocatalysis uses solid semiconductors to transform light into chemical energy. Titania is the semiconductor material considered as a universal photocatalyst due to its high activity in almost all degradation reactions concerning gas and liquid phase chemical pollutants. Titania

photocatalysts also found utility in other applications related to organic synthesis or microorganism elimination. Moreover, Titania is a material of relatively low cost and wide availability, further justifying the use of the semiconductor as the primary material in almost all applications within the photocatalytic field [2–5].

In this work we attempt to analyze the elimination of gas-phase 2-propanol using highly active titania based materials [6]. 2-propanol is a typical volatile organic pollutant present at urban atmospheres and particularly at indoor environments. Among the most typical sources of this pollutant, we can enumerate construction materials, household products, waxes, varnishes and many others [7–10]. The elimination of 2-propanol is thus of direct concern both to protect the environment as well as human health. Moreover, its elimination using photocatalysis has been frequently analyzed as a benchmark for titania materials [11–13]. The degradation of this alcohol produces a series of intermediates concomitantly observed with the total mineralization product, being

* Corresponding authors.

E-mail addresses: apodito@gmail.com (J.A. Cortés), ak@icp.csic.es, a.kubacka@icp.csic.es (A. Kubacka).

typically detected acetone, formic and acetic acids, and in some cases, formaldehyde and acetaldehyde [11–16].

The widespread use of 2-propanol as a benchmark for gas-phase testing in the photocatalytic field hasn't however drive to the rigorous analysis of the corresponding photocatalytic performance in terms of the so called true quantum efficiency, as recommended by the IUPAC [17]. According to the IUPAC definition, the calculation of the efficiency concerns the ratio between the number of molecules photo-transformed and the number of photons absorbed by the catalytic material. This calculation requires the accurate measurement of the sample surface illuminated and thus catalytically active under illumination, the light handling properties of the whole (reactor + catalyst) system to calculate the net radiation flow at the catalyst surface, as well as the catalytic properties including both activity and selectivity to obtain the number of reacting molecules as well as the number of photons (through the number of charge species used to generate the reaction products) involved in the reaction [18–23]. The efficiency observable calculation thus demands for the complete elucidation of the optoelectronic properties of the catalytic materials as well as the interaction of the solid with the radiation field at reaction conditions, that is, at the reactor where the catalytic properties are measured.

To obtain an accurate measurement of the efficiency in the photo-degradation of 2-propanol we would thus measure the reaction rate and selectivity and provide information about the reaction main intermediates and mechanism using a combination of catalytic tests and in-situ infrared spectroscopy under illumination conditions. Jointly with the analysis of the interaction of the radiation field and the reaction system they will provide the framework rendering a rigorous analysis of the efficiency through a series of titania based catalysts. These catalysts concern materials obtained at different calcinations temperatures from a single precursor. The series attempts to study the evolution of the activity occurring in parallel to the increase of the calcination temperature paying attention to the evolution of the activity, particularly when the anatase-rutile interface is present at the solid material. As well known, the presence of such interface is typically found as a critical factor to provide highly active materials in photodegradation reactions [2–5,24]. Maximum photocatalytic enhancement is typically observed in presence of relatively low quantities of rutile, between 10 and 30 mol.% [25,26]. Here we will measure such enhancement on rigorous basis (using the true quantum efficiency observable) by comparing the anatase-rutile system in a system with low quantity of rutile and a closely related anatase material obtained at a lower calcination temperature. The catalytic solids were also subjected to a basic phyco-chemical characterization of the materials using X-ray diffraction, porosity and UV-vis spectroscopy and their performance under reaction interpreted with the help of photoluminescence spectroscopy.

2. Material and methods

2.1. *TiO₂* powders preparation

Catalysts preparation was carried out in a propylene vial containing a mixture of 46.5 wt% of ethanol (Industrial grade), 8.3 wt% of titanium butoxide (Aldrich, 97.00%) and 55.3 wt% of deionized water. The mixture was transferred and heated at 200 °C under microwave irradiation by using a microwave reactor (Anton Paar, model Synthos 3000). The temperature was maintained for 2 min. The suspension obtained from the microwave reactor was atomized through a 2 mm nozzle in a YAMATO spray dryer (model DL410), at 2 bar and 200 °C. After drying, some samples received a thermal treatment (600 or 700 °C) in air during 1 h. The nomenclature used to identify the materials thermally treated was: Ti-600, Ti-700.

The Ti reference sample corresponds to the catalyst synthetized and dried by the same conditions but without subsequent thermal treatment.

2.2. Characterization

X-ray diffraction analysis was performed on a Seifert D-500 diffractometer using Ni-filtered Cu K α radiation with a 0.02 step. The average crystallite size was calculated using the Scherrer equation and the (101) anatase and (110) rutile peaks as reference. Also microstrains were measured with XRD using the Willianson–Hall formalism [27]. Specific surface area, average pore volume and size were obtained with the help of a Micromeritics equipment (model, ASAP 2010) following nitrogen adsorption at 77 K and using the Brunauer–Emmett–Teller (BET) method. Samples were degassed under flowing argon at 473 K for 2 h before nitrogen adsorption. Photoluminescence spectra were measured at room temperature on a Photoluminescence Spectrophotometer (Perkin Elmer LS50B). The optical properties of the materials (transmission or diffusive reflectance) were measured on a Shimadzu apparatus (model, UV2100) using BaSO₄ or Teflon as a reference for diffuse experiments.

Diffuse Reflectance Infrared Fourier Transform Spectra (DRIFTS) were taken in a Bruker Vertex 80 FTIR spectrometer using a MCT detector and running under OPUS/IR software. The set-up consists of a praying mantis DRIFTS accessory (Harrick Scientific) and a reaction cell (HVC, Harrick Scientific having a quartz window allowing UV-vis excitation). The reaction mixture was prepared by mixing 2-propanol (Aldrich, 99.00%; final concentration 600 ppmv) with 20 vol% O₂/N₂ flow, humidified at 90%, before entering the DRIFTS cell. The DRIFTS spectra were collected in the range of 4000–600 cm⁻¹ with a resolution of 2 cm⁻¹, by averaging 60 scans over a total of 50 s. In DRIFTS experiments in-situ light excitation was carried out using a Hg–Xe lamp and filtering the 365 nm (20 nm half-width filter; Andover) radiation.

2.3. Photocatalytic activity assessment

The photocatalytic activity of the different TiO₂ powders was evaluated by the photo-oxidation of 2-Propanol (Aldrich, 99.00%) in gas phase. The reaction was carried out in a continuous flow annular photo-reactor using a setup described elsewhere [22,28]. The amount of catalyst employed for determining the activity and selectivity for the gas-phase photo-oxidation was 40 mg. The powder was suspended in 1 mL of ethanol, which was deposited on a Pyrex tube (cut-off at ca. 290 nm), and dried at room temperature to form a thin film. The gaseous mixture (prepared before entering the reaction system) in the reactor (100 mL min⁻¹) was obtained by mixing 2-propanol (Aldrich, 99.00%; final concentration 600 ppmv) with 20 vol% O₂/N₂ flow, humidified at 90%. Under such conditions the reaction rate is independent of the organic pollutant concentration. After flowing the mixture for 4–6 h in the dark (control test), the photocatalytic experiments were carried out under UV-A light irradiation (Sylvania F6WBLT-65; 6W) or sunlight type irradiation (Philips TL54-765; 6W). Full detail of the illumination source(s) characteristics are presented in Ref. [22]. In both cases, four fluorescent lamps symmetrically positioned outside the photo-reactor were used (see configuration at supporting information section, Fig. S1). Reaction rates were evaluated under steady-state conditions, typically achieved after ca. 6–10 h from the irradiation starting. No change in activity was detected for all samples within the next 24 h and the C balance was higher than 99% in all cases. 2-Propanol and products formed were detected and quantified by gas chromatography using an on-line Agilent chromatograph (model, GC 6890) equipped with HP-PLOT-Q/HP-Innowax columns (0.5/0.32 mm I.D. × 30 m) and TCD/FID detectors.

CO_2 (measured using TCD), acetone, and formaldehyde (measured using FID) were detected in the experiments as reaction products.

2.4. Quantum efficiency formulation

The quantum efficiency is defined by Eq. (1) [17]:

$$\eta_q = \frac{\text{reaction rate} \left(\text{mol m}^{-2} \text{s}^{-1} \right)}{\text{photon rate} \left(\text{Einstein m}^{-2} \text{s}^{-1} \right)} \times 100 \quad (1)$$

It requires the calculation of the ratio between the numbers of molecules reacting (reaction rate normalized by the catalytic area) by the number of photons interacting with the catalyst. The reaction rate calculation procedure has been described in previous publications and requires the measurement of the illuminated surface area, which in turn depends on the optical and morphological properties of the sample [17,29]. One of the most common simplifications dismisses that a different number of charge carriers are required to produce different reaction products. In this situation, the denominator of Eq. (1) is approximated by the local superficial rate of absorption of photons [17,30,31]. This is obviously a simplification of the chemical situation which can be improved including a Selectivity factor (S) in the definition of the Photon rate (Eq. (2)).

$$\langle \text{photon rate} \rangle = e^{a,s}(\underline{x}) S \quad (2)$$

In Eq. (2), $e^{a,s}(\underline{x})$ is the local superficial rate of photon absorption and can be calculated using the Eq. (3).

$$e^{a,s}(\underline{x}) = q_s(\underline{x}) F_{A_s} \quad (3)$$

In this equation $q_s(\underline{x})$ is the local net radiation flux on the catalytic film and F_{A_s} is the light fraction absorbed by the sample. The flux on the film is calculated with the help of Eq. (4):

$$q_{n,\lambda}(\underline{x}) = \underline{n}_G \underline{q}_\lambda = \int_{\Omega} I_\lambda(\underline{x}, \underline{\Omega}) \underline{\Omega} \cdot \underline{n}_G d\Omega \quad (4)$$

Where \underline{n}_G is the outwardly directed unit vector normal to the catalytic film and I_λ is the intensity associated to a beam of rays carrying energy of wavelength λ in the direction of the solid angle unit vector $\underline{\Omega}$ (see full details for the calculation procedure in the Supporting information).

The dimensionless S Factor is defined by the Eq. (5).

$$S = \sum_i n_i S_i \quad (5)$$

In this equation, i runs over all products of the reaction, S_i and n_i are the fractional selectivity to product i , and the inverse of number of charge carrier species required to obtain the specific i product [6,22]. This formulation of the S Factor has a relatively simple application. In spite of it, we will show that 2-propanol displays specific features derived from the presence of reaction products produced simultaneously.

A similar equation (Eq. (6)) can be used to determinate the apparent quantum efficiency (η_{App}). In this case, according to the IUPAC recommendation [17], the denominator of the equation is the radiation flux impinging on the catalytic film (q_s).

$$\eta_{App} = \frac{\text{reaction rate} \left(\text{mol m}^{-2} \text{s}^{-1} \right)}{q_s S \left(\text{Einstein m}^{-2} \text{s}^{-1} \right)} \times 100 \quad (6)$$

3. Results and discussion

3.1. Structural and electronic characterization

In Fig. 1 we display the XRD patterns of the three samples under study. The dried sample presents, as expected, a relative widening

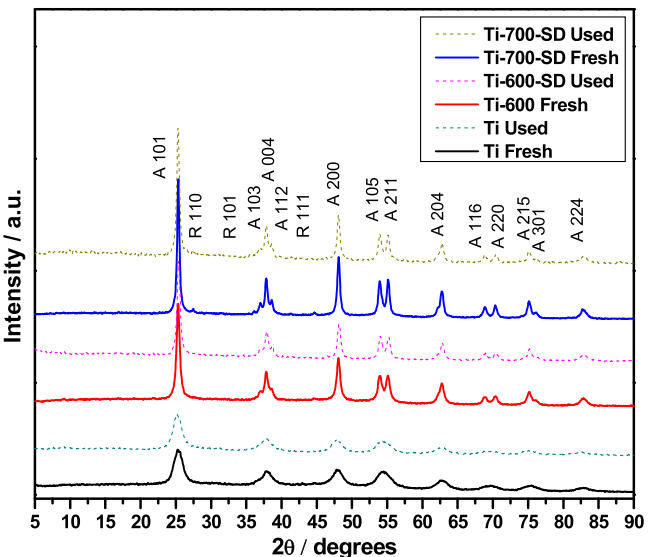


Fig. 1. XRD patterns of the fresh and used samples.

of the diffraction peaks with respect to the other samples, indicating a lower primary particle size. The width of the diffraction peaks displayed in Fig. 1 decreases in parallel to the increase of the calcination temperature. The sample patterns are dominated by the anatase polymorph profile (PDF 21-1272; space group $I4_1/\text{amd}$) and only a small quantity of rutile (PDF 21-1276; space group $P4_2/\text{mnm}$) can be detected for the sample calcined at the highest temperature. The triggering of the anatase to rutile phase transition above 600°C is a well established phenomenon in titania samples [32,33]. The anatase and rutile content of the materials (calculated using the method of Zhao and coworkers; Ref. [34]) as well as the corresponding cell parameters and primary particle size of each phase are presented in Table 1. Rutile is present in our sample calcined at 700°C in a concentration range leading to maximum photoactivity according to previous publications [25,26]. As mentioned, the primary particle size of anatase grows from ca. 6 to 22 nm within our sample series while the rutile phase appears with a particle size of ca. 35 nm (Table 1). The increasing primary particle size parallels the decrease of BET surface area and pore volume summarized in Table 2. The most significant variation occurs from the dried, non calcined sample to the first calcination analyzed. Less important although measurable variations occur between the two calcinations temperatures tested. We will use the sample calcined at 600°C , containing pure anatase as the single component, as a reasonable reference to measure the influence of the anatase-rutile interface in the photo-degradation of 2-propanol. Of course such comparison requires the use of adequate, normalized observables, such as the surface area normalized reaction rate to carry out a meaningful study.

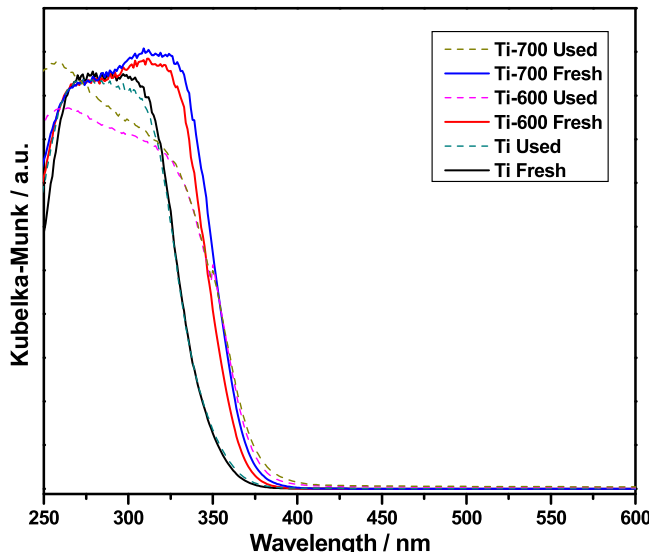
Analysis of optical properties of the samples was carried out using UV-vis spectroscopy. The corresponding optical spectra are shown in Fig. 2 for the tree samples under study. These spectra are dominated by the semiconductor decay curve at energies close to the band gap energy. The characteristic influence of the quantum confinement effect dominates the differences observed between samples [32]. As the primary particle size increases the band gap energy decreases producing a shift to higher wavenumbers in the UV-vis spectrum. The calculation of the band gap energy assuming the materials as indirect gap semiconductors [32] is presented in Table 2. Differences among samples in the band gap energy are within 0.15 eV and thus are of moderate magnitude. In any case, the variation in band gap energy through the sample series follows the trend expected from quantum confinement, quantifying the

Table 1Anatase/Rutile ratio, crystal size, microstrain, TiO_2 anatase cell parameters and TiO_2 rutile cell parameters obtained from XRD patterns.^a

Sample	Anatase/Rutile Conc. (%)		Crystal size (nm)		Anatase cell parameters		Rutile cell parameters	
	A	R	A	R	a (Å)	c (Å)	a (Å)	c (Å)
Ti	100	–	5.6	–	3.794	9.464	–	–
Ti-600	100	–	15.4	–	3.787	9.505	–	–
Ti-700	90.1	9.9	21.9	35.5	3.784	9.515	4.603	2.953

^a Average standard error; Phase conc. 9%; size 7.6%; parameters 0.3%.**Table 2**BET surface area, pore volume, pore size obtained from porosity measurements and band gap (fresh and used samples) from optical measurements.^a

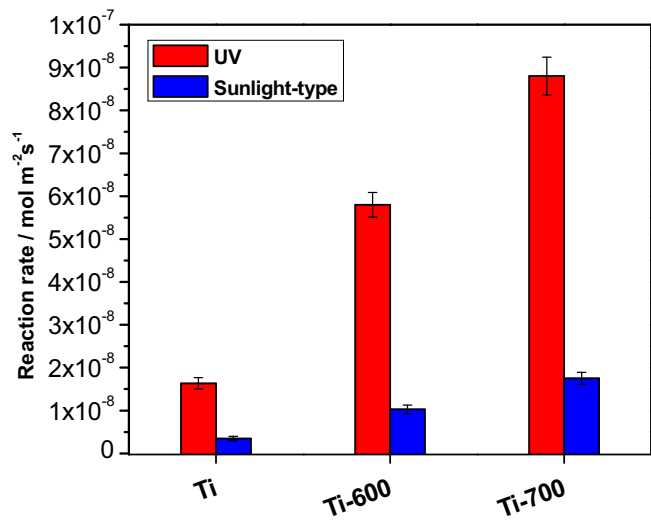
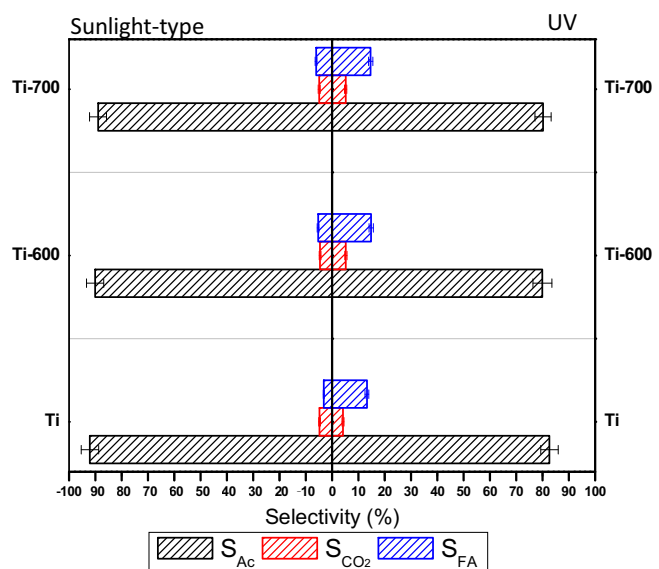
Sample	BET surface area ($\text{m}^2 \text{ g}^{-1}$)	Pore volume ($\text{cm}^3 \text{ g}^{-1}$)	Pore size (nm)	Band Gap (Fresh, e ^{−V})	Band Gap (Used, e ^{−V})
Ti	212.6	0.284	4.0	3.24	3.23
Ti-600	70.3	0.169	7.6	3.20	3.18
Ti-700	48.2	0.119	7.9	3.16	3.14

^a Average standard error; BET 1.7 $\text{m}^2 \text{ g}^{-1}$; pore size 7%; Band gap 0.04 eV.**Fig. 2.** UV-vis spectra of the fresh and used samples.

predicted decrease as calcination temperature and primary particle size increase.

3.2. Activity, selectivity and stability of the catalysts

The photocatalytic performance of the sample is first analyzed in terms of the reaction rate. As shown in **Fig. 3**, we tested the performance of the samples under UV and Sunlight-type illumination conditions. In both cases, the rates increase monotonically with the calcinations temperature or in other words with the crystallinity of the materials. This is an expected result, previously reported in a significant number of publications and summarized in specialized reviews [2,3]. The surface area normalized reaction rates (used in Eq. (1)) are presented in **Fig. 3** for all illumination sources here tested; significantly higher values are observed under UV illumination than sunlight-type. The large band gap of titania, with energy in the UV region, is the main origin of the efficient use of the UV with respect to visible light and thus of the high performance achieved in the first case [6,22]. We note that the Ti-700 reaction rate exceeds the one of the P25 reference sample by a factor of ca. 4.5 (P25 data obtained using the same experimental set-up and conditions were previously reported in Ref. [35]). The selectivity of the photodegradation reaction is on the other hand showed in **Fig. 4**. Three compounds are obtained as reaction products for the three samples studied. Two of them are

**Fig. 3.** 2-propanol degradation reaction rate under UV and Sunlight-type illumination.**Fig. 4.** Selectivity of the 2-propanol degradation under UV and Sunlight-type illumination. Reaction products: acetone (Ac), carbon dioxide (CO₂) and formaldehyde (FA).

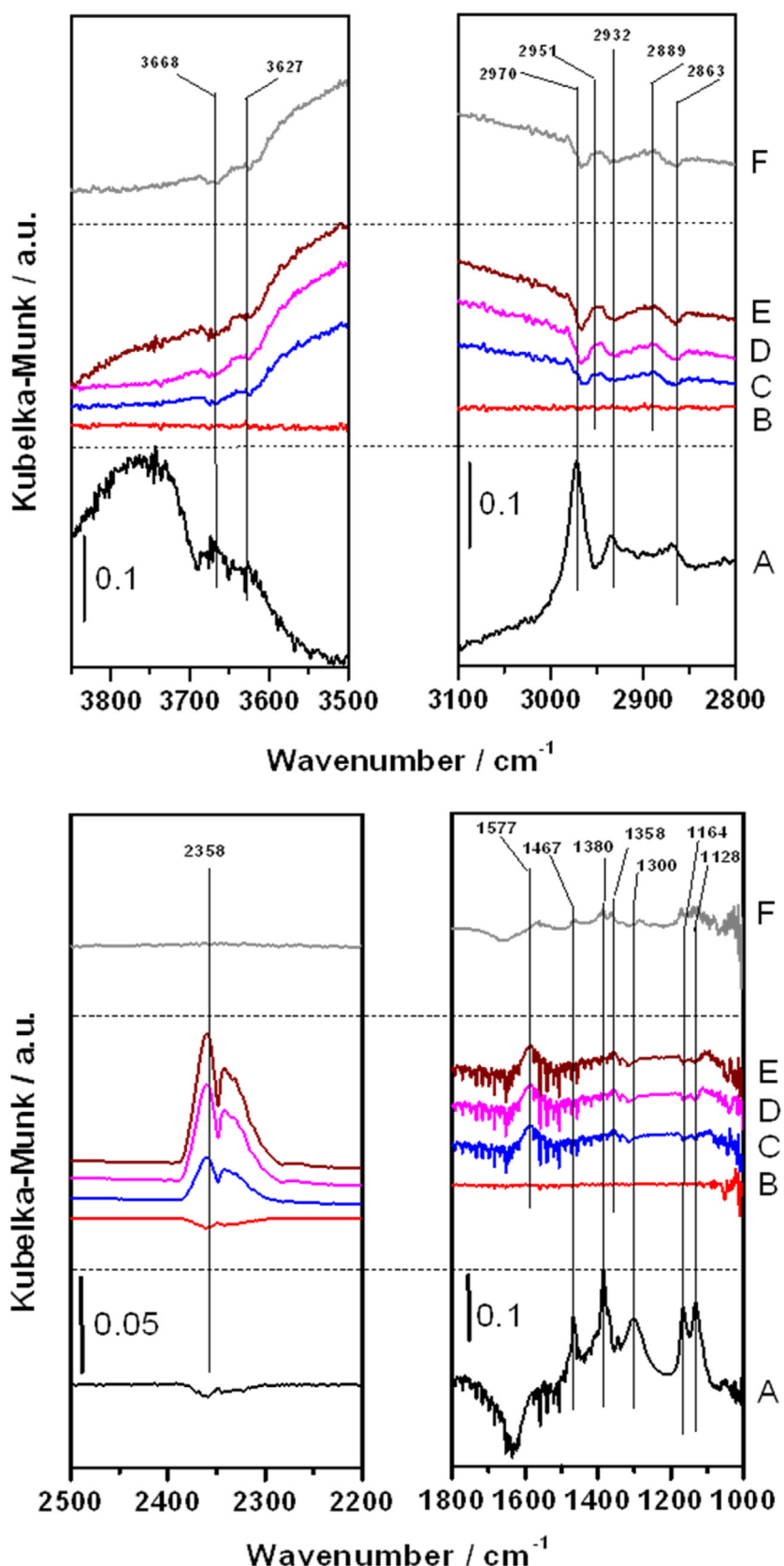


Fig. 5. DRIFTS spectra for the in-situ analysis of the 2-propanol photo-transformation occurring under reaction conditions for the Ti sample. Spectra obtained during saturation with the alcohol, under reaction-illumination conditions and subsequently at dark conditions are separated by dotted lines. A) 30 min saturation; B) initial spectrum under reaction; C-E) 20, 40, and 60 min under reaction; F) 30 min at dark.

usually obtained, acetone and carbon dioxide, while the third one is less frequently observed as is here identified as formaldehyde [11–16]. Minute differences are observed among the samples of our series in selectivity under all illumination conditions tested. More significant differences are observed when comparing UV and Sunlight-type selectivities for the same sample, indicating that the energy of the charge carrier species can modulate the selectivity observable. In fact, when comparing the two illumination sources, we observed a moderate increase of selectivity in acetone and contaminant decrease in formaldehyde production when going from UV to Sunlight-reaction. It thus seems that the charge carrier hot species may have a rather specific action in the possible evolution of acetone species.

It is important to note the fact that the catalysts are reasonable stable under reaction conditions. We tested the stability under UV and Sunlight-type illumination conditions. In Figs. 1 and 2 we also include the UV used materials XRD patterns and UV-vis spectra, respectively. No significant differences are observed between fresh and used samples. The XRD patterns and therefore primary particle size are essentially unperturbed during reaction (Fig. 1). The stability of the anatase and (when present) rutile phases for all catalysts under reaction conditions is demonstrated. Similarly, the band gap energy, measured as previously indicated, is essentially unperturbed under reaction (Fig. 2 and Table 2). Similar results are obtained when testing Sunlight-type used materials (results not shown). Both (diffraction and optical) tests provide evidence that the evolution of the catalysts under reaction conditions is rather limited (in fact unnoticeable with the techniques applied) and can be considered of low significance to discuss the photo-activity of the materials.

3.3. Calculation of the efficiency parameter

To discuss photo-activity a first point is the measurement and calculation of the true quantum efficiency. As described in the introduction and mathematically presented in Eq. (1), this requires the measurement of the reaction rate (Fig. 3) as well as the measurements of the number of photons absorbed by the catalyst. This leads to the presence of one term in the numerator of Eq. (1) and two terms in the denominator. Thus the calculation of the denominator requires the measurement of the local superficial rate of photon absorption as well as the number of charge species consumed by each product of the reaction. The latter in turn takes into account how many photons are used to convert a molecule of the reactant, 2-propanol.

3.3.1. Photon absorption by the catalysts

The local superficial rate of photon absorption mathematical description and computation procedure is described in the supporting information section. This observable in turn requires the measurement of the optical properties of the sample(s) and the net radiation flux at the catalysts surface according to equation S1. Here we consider all main optical (absorption, reflectance) events occurring at each component of the reaction system (reactor + catalyst) to carry out the calculation of the net radiation flux. The values of such observable at the catalyst surface and the local superficial rate of photon absorption for our samples are presented in Table 3. As may be expected for titania samples produced from the same precursor and thus having relative similitudes in (optical and morphological) physico-chemical properties, the net radiation flux only differs by less than 5% among our samples under both illumination conditions tested. More important differences within the sample series, amounting up to 50%, are observed in the local superficial rate of photon absorption. These differences mostly as reflect dif-

ferences in the absorbance/reflectance fraction displayed by the samples (see Fig. S6 at the supporting information section).

3.3.2. Selectivity factor

The second term of the denominator in Eq. (1) requires the calculation of the selectivity factor as mentioned previously. To provide some information about the mechanism of the reaction we carried out an in-situ IR experiment under relevant reaction conditions and interpret result using literature reports. In Fig. 5 we presented the infrared results for the Ti sample. The panels presenting specific wavenumber regions displaying difference spectra (using as reference the one obtained at time equal to zero for each treatment step) obtained during the following treatment; i) adsorption of 2-propanol at dark conditions in presence of moisture; ii) subsequent reaction under illumination conditions; and iii) post-reaction at dark conditions in presence of the reaction mixture. The adsorption of the pollutant displaces the OH-related (hydroxyls and water molecules) species at the Ti surface (see regions 3800–3500 and 1700–1600 cm⁻¹) and becomes adsorbed at the surface. Adsorption of 2-propanol generates bands at 2970, 2932, 2863 (γ_{CH_3}), 1458 (δ_{asCH_3}), 1380 (δ_{scCH_3}), 1301, 1249 (δ_{OH}), 1162 ($\gamma_{\text{C-C}}$), and 1126 ($\gamma_{\text{C=O}}$) cm⁻¹ [11,12,36–38]. Simultaneous presence of weakly adsorbed or physisorbed 2-propanol and strongly adsorbed (chemisorbed) propoxy type species is evidenced by the γ_{CH_3} and δ_{OH} vibrational modes. Typically the molecules chemisorbed at the first layer (in direct contact with titania) are in continuous exchange with physisorbed molecules located at further layers away from the solid surface. After the illumination of the sample, we observe negative bands corresponding to the consumption of 2-propanol species and the appearance of new bands at 2952, ~2889, 1661, 1577 cm⁻¹. Although these bands can be indicative of acetone formation, the most characteristic peak (ca. 1660 cm⁻¹; $\delta_{\text{C=O}}$) appears on top of a broad bump produced by changes in water population at the titania surface. These changes (i.e. water generation and/or accumulation) are independently evidenced by the changes detected in the region of coupled OH vibrations (below 3600 cm⁻¹). We can also note that the 1577 (γ_{asOCO}) and 1347 cm⁻¹ (γ_{socO}) peaks are strongly indicative of the presence of formate species [36,39,40]. As described in previously publications, the population of photocatalytic degradation products at the titania surface is severely hindered by the 2-propanol strong absorption, rendering rather low coverages which make difficult their identification. In spite of it, all works agree that acetone is the primary product in the degradation of 2-propanol in the way to carbon dioxide [11,12,14,36,41]. The total oxidation product of the photodegradation is also detected in our experiment at the ca. 2350 cm⁻¹ region. After reaction the titania surface seems to maintain essentially the same state at dark conditions.

The infrared study of the most active Ti-700 samples is presented in Fig. 6. The adsorption of 2-propanol occurs in a similar way than the presented in Fig. 5 for the Ti sample. However, significant differences are observed at the surface of the titania catalyst under illumination conditions. Concomitantly to the disappearance of 2-propanol we observe positive bands at 1577 (γ_{asOCO}) and 1358 cm⁻¹ (γ_{socO}) pointing out to the presence of formate species. This molecule alters the shape of the infrared spectrum around 2950 ($\gamma_{\text{asOCO}} + \delta_{\text{CH}}$) cm⁻¹ and contributes to the 2870 ($\gamma_{\text{C-H}}$) 2735 ($\gamma_{\text{socO}} + \delta_{\text{CH}}$) peaks [39]. In addition, we observed formation of gas phase CO₂. We can also note the presence of other intermediates leading to the band at ca. 2830 cm⁻¹, likely point out to the presence of formaldehyde or similar species [11,12,42]. The absence of accumulation of water at the surface under reaction (see regions at 3800–3500 and 1700–1600 cm⁻¹) is another difference with the Ti sample.

Thus differences among the samples as documented by the infrared study indicate that the calcination may increase the

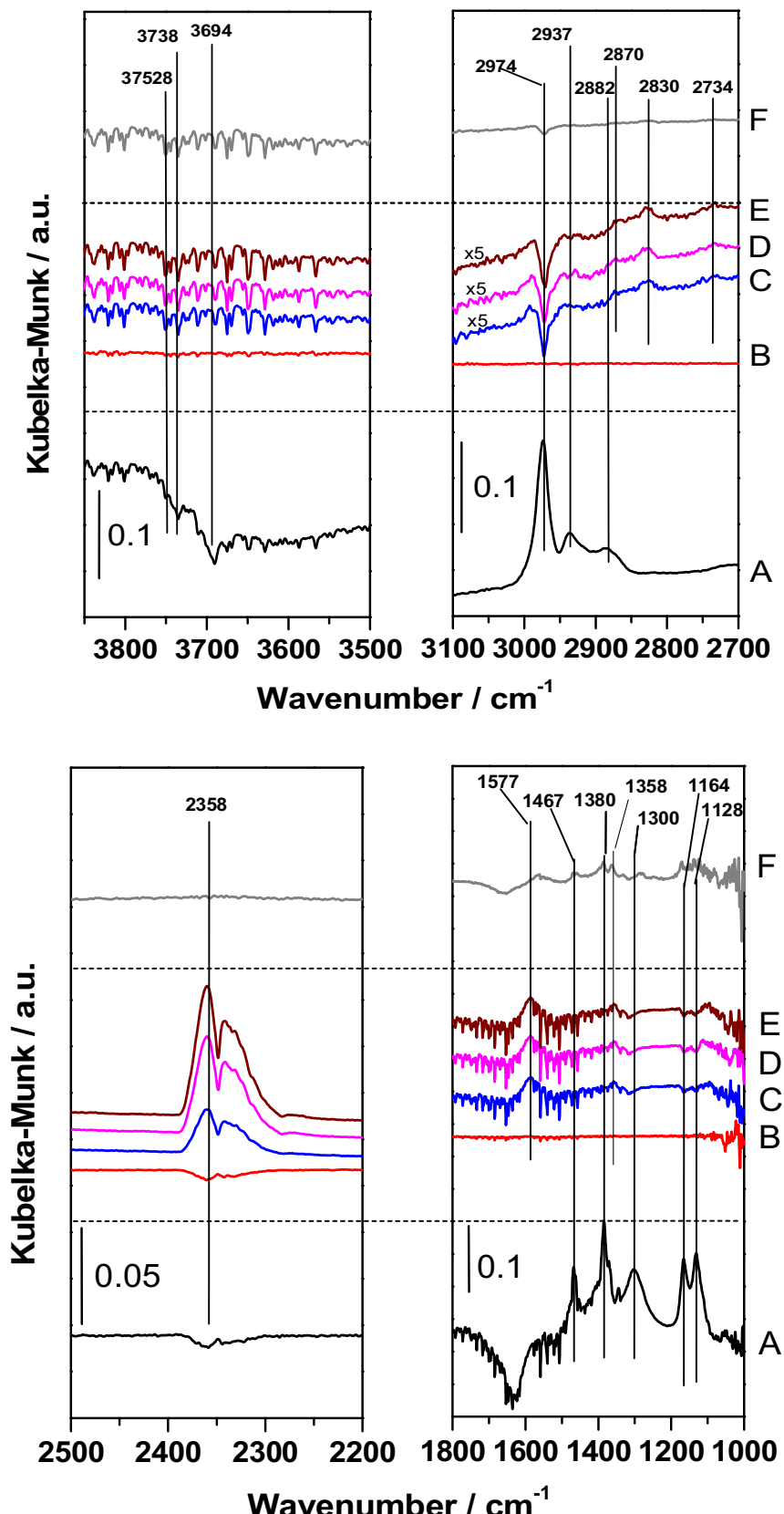


Fig. 6. DRIFTS spectra for the in-situ analysis of the 2-propanol photo-transformation occurring under reaction conditions for the Ti-700 sample. Spectra obtained during saturation with the alcohol, under reaction-illumination conditions and subsequently at dark conditions are separated by dotted lines. A) 30 min saturation; B) initial spectrum under reaction; C-E) 20, 40, and 60 min under reaction; F) 30 min at dark.

Table 3

Reaction rate, net radiation flux, local superficial rate of photon absorption, selectivity factor, and apparent and (true) quantum efficiency values obtained for the two illumination sources of the study.^a

	Rate (mol m ⁻² s ⁻¹)		q _s (Einstein cm ⁻² s ⁻¹)		e ^{as} (Einstein cm ⁻² s ⁻¹)		S Factor	
	UV	ST	UV	ST	UV	ST	UV	ST
Ti	1.6 × 10 ⁻⁸	3.5 × 10 ⁻⁹	1.2 × 10 ⁻⁸	5.2 × 10 ⁻⁸	9.0 × 10 ⁻⁹	5.9 × 10 ⁻⁹	1.62	1.79
Ti-600	5.8 × 10 ⁻⁸	1.0 × 10 ⁻⁸	1.2 × 10 ⁻⁸	4.9 × 10 ⁻⁸	8.5 × 10 ⁻⁹	4.8 × 10 ⁻⁹	1.61	1.81
Ti-700	8.8 × 10 ⁻⁸	1.8 × 10 ⁻⁸	1.2 × 10 ⁻⁸	5.0 × 10 ⁻⁸	5.5 × 10 ⁻⁹	2.6 × 10 ⁻⁹	1.67	1.85
App.QE (%) ^b		App.QE (%) ^c		QE (%) ^b		QE (%) ^c		
UV	ST	UV	ST	UV	ST	UV	ST	
Ti	8.5 × 10 ⁻³	3.7 × 10 ⁻⁴	1.4 × 10 ⁻²	6.6 × 10 ⁻⁴	1.1 × 10 ⁻²	3.3 × 10 ⁻³	1.8 × 10 ⁻²	5.9 × 10 ⁻³
Ti-600	3.0 × 10 ⁻²	1.2 × 10 ⁻³	4.9 × 10 ⁻²	2.1 × 10 ⁻³	4.2 × 10 ⁻²	1.2 × 10 ⁻²	6.8 × 10 ⁻²	2.2 × 10 ⁻²
Ti-700	4.5 × 10 ⁻²	1.9 × 10 ⁻³	7.5 × 10 ⁻²	3.5 × 10 ⁻³	9.6 × 10 ⁻²	3.7 × 10 ⁻²	1.6 × 10 ⁻¹	6.8 × 10 ⁻²

^a Average standard error; rate 4.9%; q_s 3.8%; e^{as} 5.3%; S 6.4%; App. QE 14.7%; QE 21.3%.

^b With S Factor.

^c Without S Factor.

hydrophobicity of the surface (as measured by water adsorption under illumination) and has consequences in the stability of the reaction products at the surface. This may produce differences in the coverage of the reaction products in spite that they always present at rather low coverages in presence of 2-propanol. The infrared study (Figs. 5 and 6) indicates in any case the similar mechanism and the sharing of the main intermediates in 2-propanol photo-degradation for all samples here studied. The measurement of the selectivity (Fig. 3) shows the dominance of the acetone product for all samples as previously reported by many others [11–16]. As mentioned, acetone is the primary product which is further degraded to form different reaction products. In our samples, further degradation of acetone occurs with the breaking of C–C bonds, production of formaldehyde, with subsequent evolution up to carbon dioxide. Some indications of higher surface coverage of such adsorbed species (particularly aldehydes and formates) by effect of an increasing hydrophobicity are uncovered by the infrared study as the main effect to enhance their production. The common presence of formate species in all samples would indicate on the other hand that its oxidation seems critical in all cases here studied and, as proposed by others, may involve a kinetically relevant step [42]. In spite of it, we observe that calcination has a similar (and modest) effect in the yield of all reaction products evolving from acetone, including those products as carbon dioxide presumably produced from formate surface species [11,12,39,42].

Therefore, the common mechanism and main intermediates of 2-propanol evolution under illumination for all samples studies simplify the analysis of the selectivity factor in the quantum efficiency. The degradation mechanism of 2-propanol is a complex reaction that requires the involvement of hole and electron related species in the oxidation steps [11,12,43,44]. We combined these pieces of information into the chemical equations summarized in Table 4 and representing the degradation of the three products detected. Such equations include a number of holes which is proportional to the number of water molecules as well as the number of electrons that render the superoxide species from molecular oxygen, the most abundant and active radicals according to the current knowledge [11–13,43,44]. In Table 4 we note that the production of formaldehyde generates simultaneously carbon dioxide in our photocatalytic degradation experiments [45]. Thus two end routes to this molecule are considered in Table 4 and should be taken into account to measure the number of photons consumed to generate the total oxidation product.

The corresponding balance equations (also in Table 4) can be solved as a function of a single variable, n. The general solution is included in Table 5. The solution with physical meaning would consider the absence of production of protons as we did not see a

significant evolution of the O–H bond regions under reaction conditions (see Figs. 5 and 6). No accumulation of other molecules than water appears obvious in the infrared study of the samples. Using thus the solution with $j=0$ we obtain the number of charge species consumed by each products and from these numbers the number of photons according to Eq. (5) considering that one photon produces a single charge carrier pair. Values of the S factor are included in Table 3. Limited variation, below 3%, is observed between our samples, being more significant those concerning the two illumination sources tested. We note that acetone can be produced with or without use of oxygen [11,12] but the absence of proton production when the molecule is a product detected at the gas phase requires the use of oxygen.

3.3.3. Apparent and true quantum efficiency

Having thus calculated all contributions to Eq. (1) we can calculate the efficiency parameter. We carried out the measurement of such observable within the two IUPAC formulations of the apparent and true quantum efficiency [17]. The apparent quantum efficiency is also called photonic efficiency. Values for the apparent and true quantum efficiency are displayed in Table 3 for our samples and illumination sources. The use of the two formulations can help to compare with previous publications as usually the apparent quantum efficiency is the only one reported. In relation to this point, we stress the fact that we use the IUPAC definition of the parameter, which is not always used in the literature. Instead, reports in the literature use the lamp intensity to carry out the calculation. In Table 3 we additionally included the values of the apparent or true quantum efficiency with and without selectivity factor, as the first is a common approximation used in the literature. On average the selectivity accounts for a decrease factor of ca. 1.6 (ca. 60% of error) in the efficiency observables presented in Table 3. This highlights the importance of this contribution for the calculation of the efficiency factor in quantitative basis.

Using the most stricter definition of the true quantum efficiency (next-to-last column of Table 3), we observe an increase of the efficiency of 8.7 and 11.2 times in going from the Ti to the Ti-700 sample under, respectively, UV and Sunlight-type illumination. The most active sample renders in any case high values for the true quantum efficiency for both illumination conditions, if compared with its performance in the degradation of other gas phase pollutants such as toluene which, as well known, is considered a though test for gas phase elimination [6]. Analyzing with other titania-based samples, we also observe high values (more than one order of magnitude) when compared with the degradation of chemical related (through the degradation pathway) molecules, such as acetone [23] or acetaldehyde [31,46]. According to the literature reports

Table 4

Chemical formulas and balance equations for production of acetone, formaldehyde and carbon dioxide from isopropanol.

Reaction	Equation System
i) $C_3H_8O + [nH_2O + knh^+] + [i(O_2 + e^-)] \rightarrow C_3H_6O + mH_2O + jH^+$	$1 + n + 2i = 1 + m$ $8 + 2n = 6 + 2m + j$ $nk - i = j$
ii) $C_3H_8O + [nH_2O + knh^+] + [i(O_2 + e^-)] \rightarrow C_3H_2O + 2CO_2 + mH_2O + jH^+$	$1 + n + 2i = 1 + 4 + m$ $8 + 2n = 2 + 2m + j$ $nk - i = j$
iii) $C_3H_8O + [nH_2O + knh^+] + [i(O_2 + e^-)] \rightarrow 3CO_2 + mH_2O + jH^+$	$1 + n + 2i = 6 + m$ $8 + 2n = 2m + j$ $nk - i = j$

Table 5General solution of equations of Table 4 and particular solution for $j = 0$.

Product	General solution	Relevant Solution Solutuionsolucion
i) Acetone	$m = n - \frac{2}{3}nk + \frac{4}{3}$ $j = -\frac{2}{3} + \frac{4}{3}nk$ $i = \frac{2}{3} - \frac{1}{3}nk$	$j = 0$ $n = i = \frac{1}{2}$
ii) Formaldehyde	$m = n - \frac{2}{3}nk + \frac{16}{3}$ $j = -\frac{14}{3} + \frac{4}{3}nk$ $i = \frac{14}{3} - \frac{1}{3}nk$	$j = 0$ $n = i = \frac{14}{3}$
iii) Carbon dioxide	$m = -nk + \frac{3}{2}n + \frac{21}{2}$ $j = -13 - n + 2nk$ $i = n + 13 - nk$	$j = 0$ $n = i = 13$

[3,25,26], the presence of a rutile concentration leading to optimum activity provides the grounds for the high activity displayed by the Ti-700 sample. To emphasize this point, we note that this sample shows a true quantum efficiency being 7.9 and 4.4 times superior to the P25 sample for, respectively, UV and Sunlight-type illumination conditions. So, the anatase-rutile contact in this sample appears far superior to the P25 reference.

To interpret the evolution of the efficiency parameter within our sample series, in Fig. 7 we plot the efficiency parameter(s) as well as its components (Eq. (1)) in a normalized version, fixing as 1 the corresponding observable for the Ti sample. The normalization is carried out to facilitate the comparison between the different physical observables contributing to the efficiency (Eq. (1)). In the first panel (of the two rows of Fig. 7; upper row UV results; lower row; Sunlight-type results) we compared the normalized apparent and true quantum efficiency with the normalized reaction rate. Inclusion of the S factor in Eq. (1) makes that the apparent and true quantum efficiencies do not mimic the trend (specifically showing different slope(s) of the corresponding, quasi-linear trends) of the rate. Normally the apparent quantum efficiency reported in the literature mimics the trend of the rate as it lacks the selectivity factor. In any case, we see that the apparent quantum efficiency and the rate mostly differ in the slope of their roughly linear trends visible displayed for the two illumination conditions tested. The true quantum efficiency shows however a non-linear trend. Such difference in the efficiency observables behavior in the sample series can be easily interpreted by looking at the other two panels of Fig. 7. Comparing the changes observed in the optical-related parameters (central panel) or the selectivity (last panel) we observe the rather limited effect of the last parameter due to the strong similitudes in selectivity showed by the samples here studied. This leads to variations in the selectivity factor of less than 3.5% (Fig. 7; last panel). Concerning the optical-related panels, as mentioned previously, there are minor changes in the net radiation flux among the catalysts (Table 3), explaining the similar trend presented by the apparent quantum efficiency and reaction rate in Fig. 7. The differ-

ences in the fraction of light absorbed leads on the other hand to strong differences in the local superficial rate of photon absorption among the samples, and thus modifies significantly the trend (particularly the slope of quasi-linear trend) when comparing the true quantum efficiency and the other two observables of the first panel of Fig. 7. So, the measurement of the optical properties of the solids and the subsequent inclusion of all optical events (transmittance-absorption and reflection) in the calculation of the efficiency makes a strong impact when comparing the differences between samples of our series.

Additionally, we can highlight the fact that the use of the apparent quantum efficiency drive to erroneous conclusion not only in quantitative terms but also when making comparison between samples of the series or, in other words, even in the case of analyzing a differential effect using a sample of the same series as reference. In particular, we focus on the comparison between the Ti-600 and Ti-700 samples to measure the effect of the anatase-rutile interface with respect to the parent anatase sample. The arrows plotted in the first panel of Fig. 7 indicate the difference between the apparent and true quantum efficiency for the Ti-600 and Ti-700 samples. The dimension of the arrows would indicate that very different results are obtained when comparing these two samples at the apparent/true quantum efficiency computation level under all illumination conditions tested. Measuring the effect of the anatase-rutile interface (as the ratio between efficiencies; i.e. Ti-700/Ti-600) renders factors of 1.5/1.6 (apparent quantum efficiency) and 2.3/3.1 (true quantum efficiency) for UV/Sunlight-type illumination. This leads to an error of ca. 55 and 95% for, respectively, UV and Sunlight-type tests of 2-propanol photo-degradation. The use of true quantum efficiency seems thus mandatory for a quantitative analysis of the performance of the samples but also to provide a relative measurement of the photocatalytic performance among them.

To fully justify the differences in efficiency of the samples we carried out a photoluminescence study of the samples under UV and visible light excitation. Fig. 8 gives the de-excitation spectra under

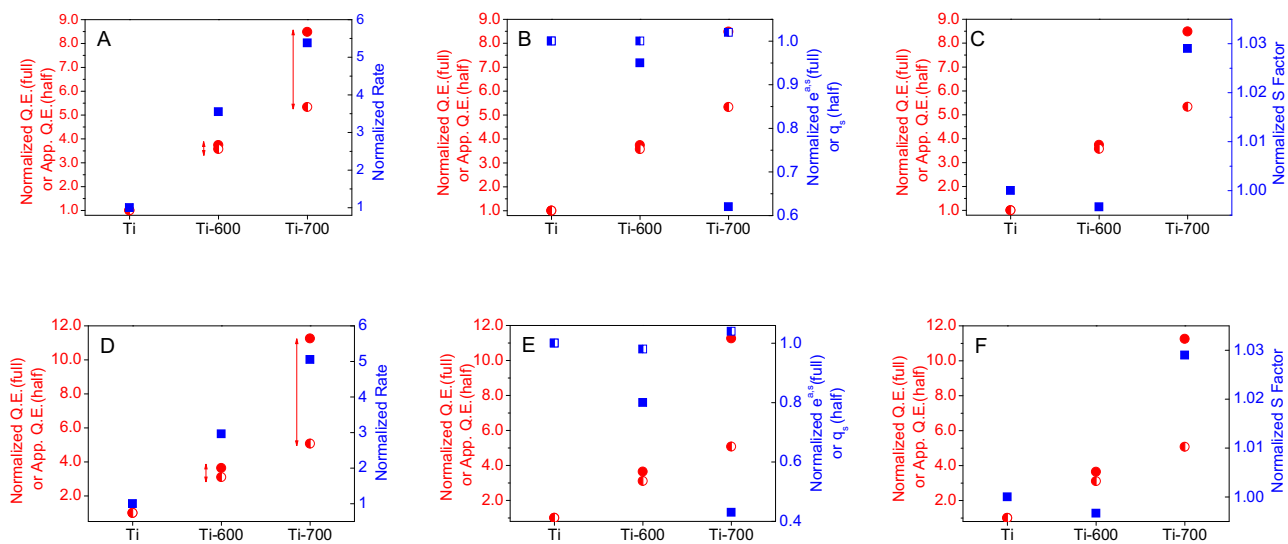
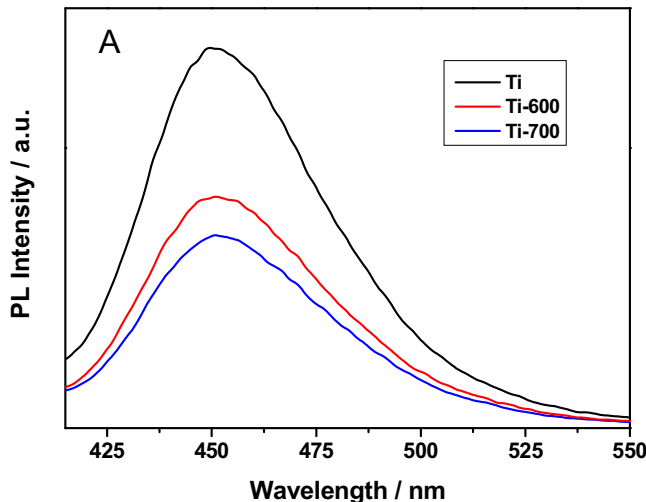


Fig. 7. Plot showing the evolution of (normalized) reaction rate, local rate of photon absorption, selectivity factor (right OY axis) and quantum efficiency (left OY axis) observables. Upper row: UV illumination (A–C); Lower row: Sunlight-type illumination (D–F).



UV (365 nm; upper panel of Fig. 8) and visible (425 nm; lower panel) irradiation. The spectra are dominated by a broad, asymmetric feature peaking at approx. 450 nm in the case of UV excitation (365 nm) and a decay feature (originated from the close proximity of the excitation line) with a rather weak peak at ca. 535 nm for the visible light excitation (425 nm). Both are characteristics of titania samples and correspond to de-excitation features concerning defects and or localized states as direct (UV-triggered) inter-band de-excitation features are rather weak due to the indirect gap nature of the semiconductor [6,47]. Due to the similar shape of the de-excitation decays, it is obvious that the samples present the same decay mechanism(s) and only differ significantly in the overall intensity. The intensity decay trend under UV and visible show some differences with a significant decrease for the calcined samples with respect to the parent Ti sample under UV. The photoluminescence intensity variation among samples under UV excitation has a direct correlation with the photocatalytic results presented in Fig. 3 and suggests that the opto-electronic catalysts response to the UV part of the electromagnetic region dominates the performance of the samples and thus has a key catalytic role under Sunlight-type illumination conditions.

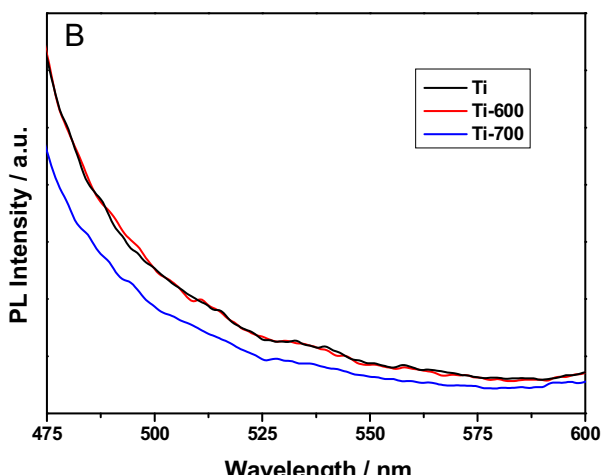


Fig. 8. Photoluminescence spectra of the sample under UV (365 nm; panel A) and Visible (425 nm; panel B) excitation.

4. Conclusions

In this work we presented a study of highly photo-active titania materials prepared by spray drying and further calcined in the 600–700 °C region. The characterization of the materials provided information about their physico-chemical properties indicating that the increasing calcination temperature produces a decrease in surface area, increase of the primary particle size of the initially present anatase polymorph as well as the presence of rutile at the highest temperature.

The analysis of the quantum efficiency shows that optimum photocatalytic performance is achieved within our series for the sample having the adequate opto-electronic properties. The maximum efficiency is achieved through the combined (as both are quantitatively important) optimization of i) the electron-hole recombination, with direct impact in the reaction rate, and ii) the adequate solid optical properties (measured and influencing efficiency through the local superficial rate of photon absorption parameter). The first (i.e. electron-hole recombination) is directly related to the effect of the anatase-rutile contact in

charge handling at the Ti-700 sample but the second (i.e. optical absorbance/reflectance) has its roots in a significant number of properties of the catalytic solid, including structure, morphology and defect characteristics.

The study also highlights the importance of analyzing the efficiency through the application of the strictest definition (i.e. the true quantum efficiency). In fact, we measure the error of the two most common simplifications in the efficiency formulation. First, the elimination of the selectivity factor drives to errors of ca. 60% in the efficiency presented by our samples in the 2-propanol degradation. Second, comparing the apparent and quantum efficiency values for analyzing the performance of the anatase-rutile contact with respect to the parent anatase sample, we measure an error of ca. 55 and 95% for, respectively, UV and Sunlight-type illumination conditions. Such errors reinforce the idea that the true quantum efficiency parameter should be the only formulation used to obtain both absolute and relative (between samples of the same series) measurements of the photocatalytic performance.

Acknowledgements

Experimental work was supported through MINECO ENE2013-46624-C4-1-R project. Uriel Caudillo-Flores acknowledges financial support from CONACYT Mexico through the Bioenergy Thematic Network ("Red Temática de Bioenergía") and CIC of UMSNH.

Appendix A. Supplementary data

Supplementary data associated with this article can be found, in the online version, at <http://dx.doi.org/10.1016/j.apcatb.2016.08.014>.

References

- [1] Environmental topics, European Environmental Agency, <http://www.eea.europa.eu/themes>, 2013 (accessed 16.05.16).
- [2] M.R. Hoffmann, S.T. Martin, W. Choi, D.W. Bahnemann, *Chem. Rev.* 95 (1995) 69–96.
- [3] A. Kubacka, M. Fernández-García, G. Colón, *Chem. Rev.* 112 (2012) 1555–1614.
- [4] L. Jing, W. Zhou, G. Tian, H. Fu, *Chem. Soc. Rev.* 42 (2013) 9509–9549.
- [5] Z. Wang, Y. Liu, B. Huang, Y. Dai, Z. Lou, G. Wang, X. Zhang, X. Qin, *Phys. Chem. Chem. Phys.* 16 (2014) 2758–2774.
- [6] U. Caudillo-Flores, M.J. Muñoz-Batista, F. Ung-Medina, G. Alonso-Núñez, A. Kubacka, J.A. Cortés, M. Fernández-García, *J. Chem. Eng.* 299 (2016) 393–402.
- [7] W.-K. Jo, K.-H. Park, *Chemosphere* 54 (2004) 565–595.
- [8] D. Kutzias, *Exp. Toxicol. Pathol.* 57 (2005) 5–7.
- [9] U.B. Celebi, N. Vardan, *Atmos. Environ.* 423 (2008) 5685–5695.
- [10] J. Gunschera, J.R. Anderson, N. Schulz, T. Salthanimer, *Chemosphere* 75 (2009) 476–482.
- [11] F. Arsac, D. Bianchi, J.M. Chovelon, C. Ferronato, J.M. Hermann, *J. Phys. Chem. A* 110 (2006) 4202–4212.
- [12] F. Arsac, D. Bianchi, J.M. Chovelon, C. Ferronato, J.M. Hermann, *J. Phys. Chem. A* 110 (2006) 4213–4222.
- [13] D. Vilduza, R. Portela, C. Ferronato, J.M. Chovelon, *Appl. Catal. B* 107 (2011) 347–354.
- [14] S.A. Larson, J.A. Widgren, J.L. Falconer, *J. Catal.* 157 (1995) 611–625.
- [15] W. Xu, D. Raferty, *J. Phys. Chem. B* 105 (2001) 4343–4349.
- [16] A. Wisthaler, P. Strou-Fejsen, L. Fang, A. Hensel, T.D. Mark, D.P. Wyon, *Environ. Sci. Technol.* 41 (2006) 229–234.
- [17] S.E. Braslavsky, A.M. Braun, A.E. Cassano, A.V. Emeline, M.I. Litter, L. Palmisano, V.N. Parmon, N. Serpone, *Pure Appl. Chem.* 83 (2011) 931–1014.
- [18] O. Alfano, D. Bahnemann, A. Cassano, R. Dillert, R. Goslich, *Catal. Today* 58 (2000) 199–230.
- [19] N. Serpone, *J. Photochem. Photobiol. A: Chem.* 104 (1997) 1–12.
- [20] L. Palmisano, V. Augugliaro, R. Campostrini, M. Schiavello, *J. Catal.* 143 (1993) 149–154.
- [21] B. Ohtani, *Chem. Lett.* 37 (2008) 216–229.
- [22] M.J. Muñoz-Batista, A. Kubacka, A.B. Hungría, M. Fernández-García, *J. Catal.* 330 (2015) 154–166.
- [23] C. Lugo-Vega, B. Serrano-Rosales, H. de Lasa, *Appl. Catal. B* 198 (2016) 211–223.
- [24] Y. Nosaka, A.Y. Nosaka, *J. Phys. Chem. Lett.* 7 (2016) 431–434.
- [25] J. Zhang, Q. Xu, Z. Feng, M. Li, C. Li, *Angew. Chem. Int. Ed. Engl.* 120 (2008) 1790–1793.
- [26] K. Wang, J.J. Chen, X. Zhang, Y.X. Huang, W.W. Li, H.Q. Yu, *Sci. Rep.* 6 (2016) 20491.
- [27] G. Williamson, W. Hall, *Acta Metall. Mater.* 1 (1953) 22–31.
- [28] M.J. Muñoz-Batista, M.N. Goímez-Cerezo, A. Kubacka, D. Tudela, M. Fernández-García, *ACS Catal.* 4 (2014) 63–72.
- [29] M.J. Muñoz-Batista, A. Kubacka, O. Fontelles-Carceller, D. Tudela, M. Fernández-García, *ACS Appl. Mater. Interface* 8 (2016) 13934–13945.
- [30] G.E. Imoberdorf, H.A. Irazoqui, A.E. Cassano, O.M. Alfano, *Photocatal. Ind. Eng. Chem. Res.* 44 (2005) 6075–6085.
- [31] M.J. Muñoz-Batista, M. de los Milagros Ballari, A. Kubacka, A.E. Cassano, O.M. Alfano, M. Fernández-García, *Chem. Eng. J.* 255 (2014) 297–306.
- [32] M. Fernández-García, A. Martínez-Arias, J.C. Hanson, J.A. Rodriguez, *Chem. Rev.* 104 (2004) 4063–4104.
- [33] M. Fernández-García, X. Wang, C. Belver, J.C. Hanson, J.A. Rodriguez, *J. Phys. Chem. C* 111 (2007) 674–682.
- [34] H. Zhang, J.F. Banfield, *J. Phys. Chem. B* 104 (2000) 3481–3487.
- [35] G. Colón, P. Sampedro, M. Fernández-García, H. Chen, J.C. Hanson, J.A. Rodriguez, *Langmuir* 24 (2008) 11111–11118.
- [36] J.M. Coronado, S. Kataoka, I. Tejedor-Tejedor, M.A. Anderson, *J. Catal.* 219 (2003) 219–230.
- [37] J. Araña, A.P. Alonso, J.M.D. Rodríguez, G. Colón, J.A. Navío, J.P. Peña, *Appl. Catal. B: Environ.* 89 (2009) 204–213.
- [38] Q. Gu, X. Fu, X. Wang, S. Chen, D.Y.C. Leung, X. Xie, *Appl. Catal. B: Environ.* 106 (2011) 689–696.
- [39] Ch. E. Nanayakkara, J.K. Dillon, V.H. Grassian, *J. Phys. Chem. C* 118 (2014) 25487–25495.
- [40] W.-C. Wu, C.-C. Chuang, J.-L. Lin, *J. Phys. Chem. B* 104 (2000) 8719–8724.
- [41] W. Xu, D. Raferty, J.S. Francisco, *J. Phys. Chem. B* 107 (2003) 4537–4544.
- [42] Z. Topalian, B.I. Stefanov, C.G. Granqvist, L. Österlund, *J. Catal.* 307 (2013) 265–274.
- [43] Y. Ohko, K. Hashimoto, A. Fujishima, *J. Phys. Chem. A* 101 (1997) 8057.
- [44] D. Brinkley, T. Engel, *J. Phys. Chem. B* 102 (1998) 7596.
- [45] D.P. Wilson, D. Sporleder, M.G. White, *J. Phys. Chem. C* 116 (2012) 16541–16552.
- [46] M.M. Ballari, J. Carballada, R.I. Minen, F. Salvadores, H.J.H. Bonwers, O.M. Alfano, *Process Saf. Environ. Prot.* (2016), <http://dx.doi.org/10.1016/j.psep.2015.008.003>.
- [47] C.C. Mercado, Z. Seeley, A. Bandyopadhyay, S. Bose, J.L. McHale, *ACS App. Mater. Interface* 3 (2011) 228–234.